

Contrôle de la pollution acoustique extérieure

Aure Abinal, Imad Amri, Nessrine Chiba, Julius Graf, Auguste Malgrain

Contents

1 TrainQuell	2
1.1 Noise pollution from trains in France	2
1.2 TrainQuell : the next step in acoustic engineering for the railway industry	2
1.3 Our strategy	2
2 State of the art	4
3 Physical background	5
3.1 Modelling train noise	5
3.1.1 Noise source	5
3.1.2 Frequencies considered	6
3.2 Choosing a suitable material	6
3.2.1 Absorption capacity	6
3.2.2 Availability of the materials	9
4 Mathematical model	11
4.1 Introduction	11
4.2 Formalization of the problem	11
4.3 Determination of $\alpha(\omega)$ for a frequency ω	12
4.4 Dirichlet condition	14
4.5 Optimizing the distribution of acoustic energy	17
4.6 Open-air boundary theoretical study	19
4.7 Optimizing β using LASSO regression and the wall shape	20
5 Numerical results	22
5.1 Optimizing β and fractal shape	22
5.2 Frequency study	26
5.3 Conclusion	27
6 Conclusion	29

Chapter 1

TrainQuell

1.1 Noise pollution from trains in France

In its latest report in October 2021, the ADEME (the french ecological transition agency) estimated the social cost of noise in France at €147.1 billion a year. Rail noise accounts for 7.6% of these costs, or €11.2 billion a year [13].

Dealing with the noise pollution generated by rail traffic is a health and social issue, as well as a significant factor in regional development. What's more, it's a subject that is subject to strict national and European regulations. Controlling rail noise is therefore essential for the proper development of the network and traffic in the years to come.

The question of the ecological impact of solutions also arises: according to the SNCF, "The reduction of noise is an opportunity for the company to innovate, while fully integrating the sustainable development objectives it has set itself"[13].

1.2 TrainQuell : the next step in acoustic engineering for the railway industry

As the world shifts gears towards greener transit, trains are increasingly favored for their lower environmental impact. TrainQuell champions this shift by creating acoustic barriers that minimize noise pollution. Our solutions are low-carbon and designed to last, and they incorporate the future challenges of rail traffic. They are meant to not only protect community tranquility but also support the natural habitats alongside railways. We're paving the way for trains to be the preferred choice for travel and freight, contributing to a sustainable and serene future.

1.3 Our strategy

Our strategy concentrates on the development of innovative, non-planar acoustic walls, embedded with absorptive materials, specifically targeting the effective dissipation of sound waves emanating from railways.

The key elements of our strategy include:

- **Innovative Design:** Employ advanced numerical methods to engineer ϵ -optimal wall shapes. These designs are aimed at significantly reducing noise within specific frequency ranges, particularly in reflective tunnel environments.

- **Strategic Partnerships:** Establish a collaborative relationship with SNCF in France to test and refine our solutions in real-world scenarios. Following successful implementation, we plan to expand into the German market and, subsequently, across Europe.
- **A solution for the long term:** Trains are travelling at increasingly high speeds, with TGVs today sometimes travelling at speeds of 320 km/h. Beyond 300km/h, two noises are perceptible: the vibration noise of the tracks and the aerodynamic noise of the train, both in different frequency ranges. Current solutions on the market, however, focus on the first source, ignoring aerodynamic noise, which will only increase with train speed. Our solution aims to attenuate both these noises, which sets us apart from our competitors. We would also like our solution to be materially resistant, so that it lasts as long as possible.
- **Eco-designed materials:** Our strategy is part of a global reflection on impact. We're aiming to implement our solution using bio-sourced materials that require little water and energy to manufacture.

Chapter 2

State of the art

The study of noise emitted by trains has been a subject for engineers since the boom in train use. Ever since the introduction of the steam engine, there has been talk of dealing with the noise made by these machines. The technological improvements that trains have undergone have already made it possible to reduce train engine noise.

Nowadays, however, trains still make too much noise, especially when travelling at high speed. What's more, railway lines often run close to towns or residential areas, so their noise pollution needs to be controlled. Numerous solutions have been proposed to control this noise, particularly at wheel level, since this is where there are the most sources of noise (friction and squealing against the rail).

The company Strail ([14]) offers an innovative solution of noise barriers placed very close to the wheels, which are fixed to the track. These rubber acoustic barriers absorb the noise of the wheels as they rub against the rail.

However, when an acoustic barrier is placed next to a railway line, which itself is placed next to housing (a residential area containing roads), the noise from the cars reverberates against the acoustic barrier, becoming just as annoying as the noise from the train that we wanted to limit. To solve this problem, Réseau Ferré de France ([1]) has innovated with a double-sided acoustic wall that absorbs both train noise and traffic noise on either side of the wall.

Another way of optimising the control of noise pollution is to create irregularities in the wall surface. This was done for interior barrier, especially by RPG Europe [2]: this company creates fractal walls for acoustic rooms. It was Marcel Filoche's work that led to the development of walls whose surface represents a fractal. This type of pattern would increase the surface area in contact with the air while using very little material. His works have lead to the construction of fractal acoustic barriers by Colas [11] at the turn of the century. These acoustic barriers are placed close to motorways and railway lines.

Improving that level of fractal in order to optimize the use of the material could be the part where our start-up stands out from these previous innovations.

Chapter 3

Physical background

3.1 Modelling train noise

3.1.1 Noise source

Railway noise is mainly due to three sources (comparison provided in [3.1](#)):

- Equipment noise: this comes from engines, fans and air conditioning. It occurs mainly at low speeds and when stationary.
- Rolling noise: this results from the contact of the wheels on the rail and the microscopic irregularities present on their surfaces. This is the main source of noise at normal speeds.
- Aerodynamic noise: this is caused by the train entering the air. It is perceived from 300 km/h, and becomes the main source of noise above 320 km/h. [\[13\]](#)

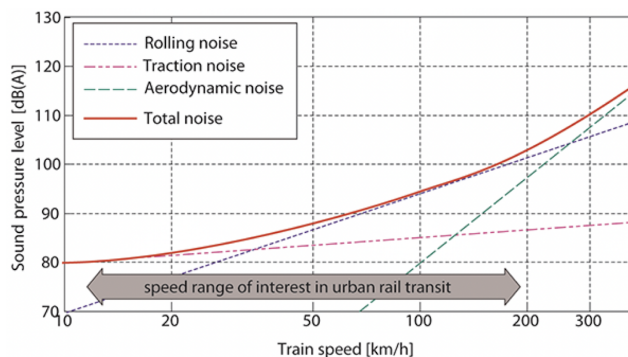


Figure 3.1: Preponderance of airborne noise sources as a function of train speed. Source : K. Vogiatzis & G. Kouroussis, 2017. voir [\[3\]](#)

It should be noted that trains currently run in France at speeds of up to 320km/h, but not above. However, this is the case in Japan, where some trains regularly travel at 500km/h, in Italy (360km/h) or in China (up to 430km/h)[\[5\]](#). It therefore seems reasonable to assume that French trains will soon be running at higher speeds, generating significant aerodynamic noise.

We are therefore concentrating on two sources: rolling noise and aerodynamic noise.

3.1.2 Frequencies considered

The rolling noise of a railway track results from the interaction between the rolling stock and the infrastructure (wheel/rail contact). Trains with very different characteristics (size, mass, materials, wheel roughness, etc.) run on the same track, each with its own "acoustic signature" [12]. We therefore need to consider a wide frequency range for this noise, estimated at between 400 and 4000 Hz [15], and so the pulse $\omega \in [2500, 25000]$ approximately.

We also want to estimate the frequency of the aerodynamic noise of a train. To do this, we will look at the spectrum of a sound signal corresponding to a TGV passing by.

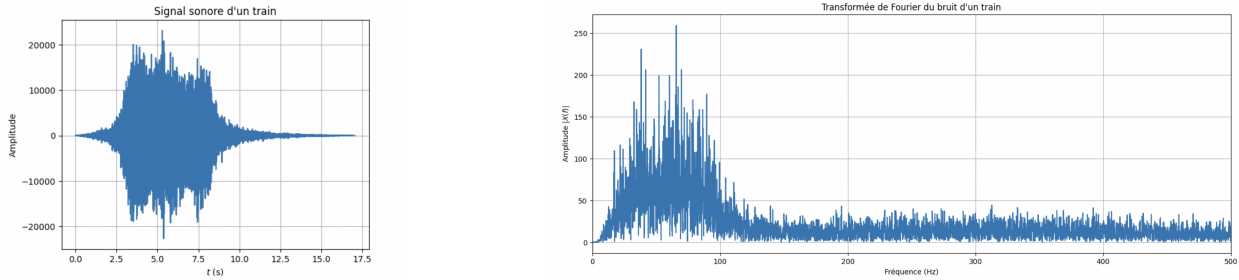


Figure 3.2: Train noise analysis

By 3.2, the frequency range $[15, 110]$ Hz is assumed, which correspond to $\omega \in \underline{\omega} := [100, 700]$ rad/s approximately.

3.2 Choosing a suitable material

To draw up a coherent proposal for our acoustic barrier, we need to look at the material to be used. The aim of the problem is to study not only the distribution of the absorbent material on the wall, but also (and above all) the nature and acoustic properties of the material.

3.2.1 Absorption capacity

Initially, this study is based on an examination of the physical parameters of the materials. The comparison of the different materials therefore begins with a study of the Robin conditions imposed at the wall (the boundary between the wall and the tunnel). This boundary condition is written as :

$$\frac{\partial u}{\partial n} + \alpha u = 0$$

As defined in the Chapter 3 of the handout, α is a complex coefficient that gives information about the absorption of the given material. Its complex arguments give information about physical phenomena inside the material. They are set as $\Re(\alpha) > 0$ and $\Im(\alpha) < 0$.

$\Re(\alpha)$ is related to the absorption phenomena. It appears that the larger $\Re(\alpha)$, the better the soundproofing properties of the material. In the same way, $\Im(\alpha)$ deals with the phenomena of reflexivity of the acoustic wave. The larger $\Im(\alpha)$, the better the wave's reflexion. However, for the purpose of our study, it would be interesting to compare the absorbency of a material with its reflectivity. To do this, we will look at the ratio between the real part and the imaginary part. The greater this ratio (in absolute terms), the more suitable the material will be for our tunnel, as its absorbency will outweigh

its reflectivity.

We can use the Python function established in the project of the theoretical path to compute α (see chapter 4). This function calculates the correct value of α for a given material. It uses as arguments the pulsation ω , and also internal characteristics of the material : the porosity Φ , the tortuosity α_h and the resistivity to the passage of air σ . The final argument is also the function g , which corresponds to the function associate with the limit condition. For the study of the suitable material, we take a simple function g but next chapters will attach importance to correct modelling of g .

It is important to note that the calculation of alpha depends on the study pulsation. Therefore, we will find different α depending on the pulsation we consider in our study.

That being said, we can plot $\frac{\Re(\alpha)}{\Im(\alpha)}$ for different materials and study what are the results for the computation of α . We found several materials using the handout of theoretical path, and also materials given in [6] and in [4].

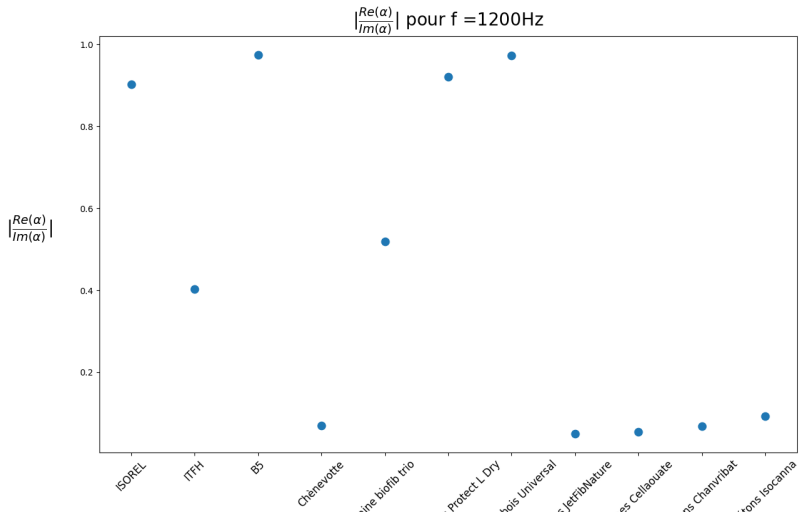


Figure 3.3: Results on $\left| \frac{\Re(\alpha)}{\Im(\alpha)} \right|$ depending on the used material for $f = 1200$ Hz

Using the arguments given in the previous part, we plot results for different pulsations. Indeed, we are studying different noises, with different origins, who are led by different pulsations. The previous study (for $f = 1200$ Hz, see 3.3) was held for the noises due to equipment and rolling. They are the most predominant noises for the majority of the trains. Nevertheless, when the train gets to high speeds, we should consider also aerodynamic noise (it even becomes predominant when speed exceeds 320 km/h). This noise is produced with a much lower frequency (≈ 100 Hz). We can thus study what is the best material for this frequency too (see 3.4)

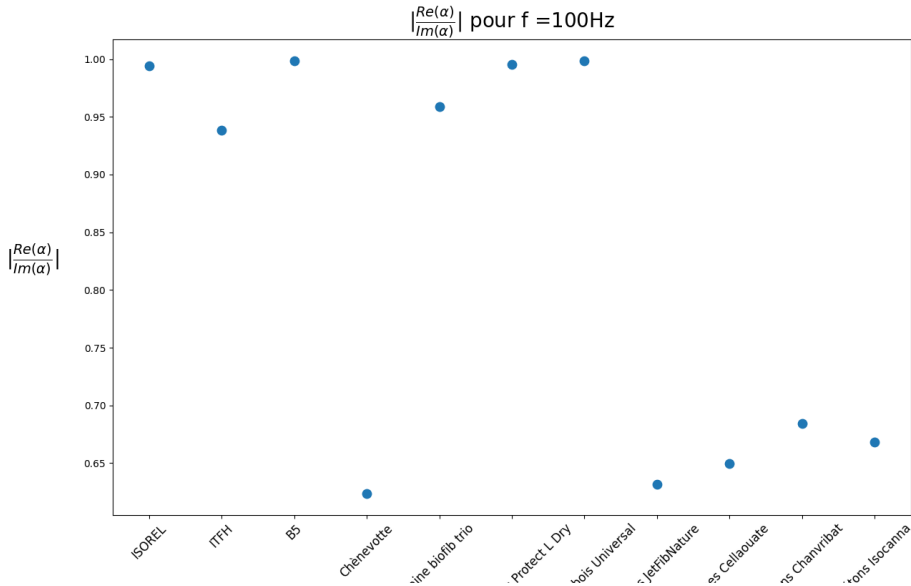


Figure 3.4: Results on $\left| \frac{\Re(\alpha)}{\Im(\alpha)} \right|$ depending on the used material for $f = 100$ Hz

For the two different graphs, we can extract several materials that could work for our acoustic barrier (the highest ratios). We can then plot the values taken by $\frac{\Re(\alpha)}{\Im(\alpha)}$ for the considered materials on the two frequency ranges of interest to us (see 3.5 and 3.6).

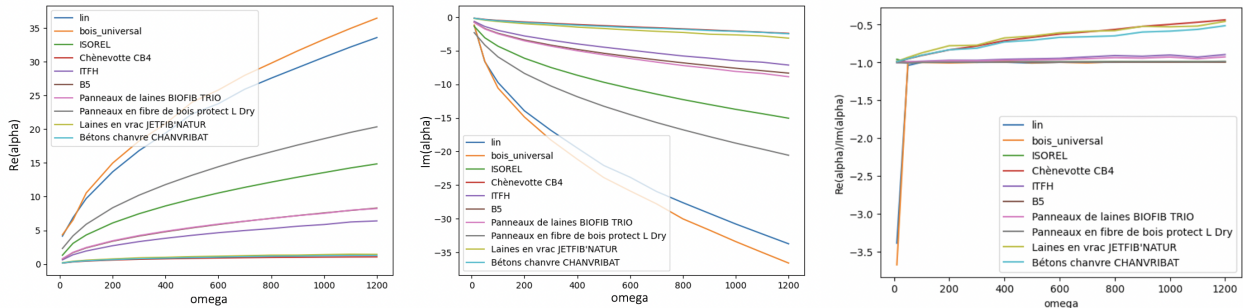


Figure 3.5: Results on $\left| \frac{\Re(\alpha)}{\Im(\alpha)} \right|$ depending on the used material for a low-frequency system

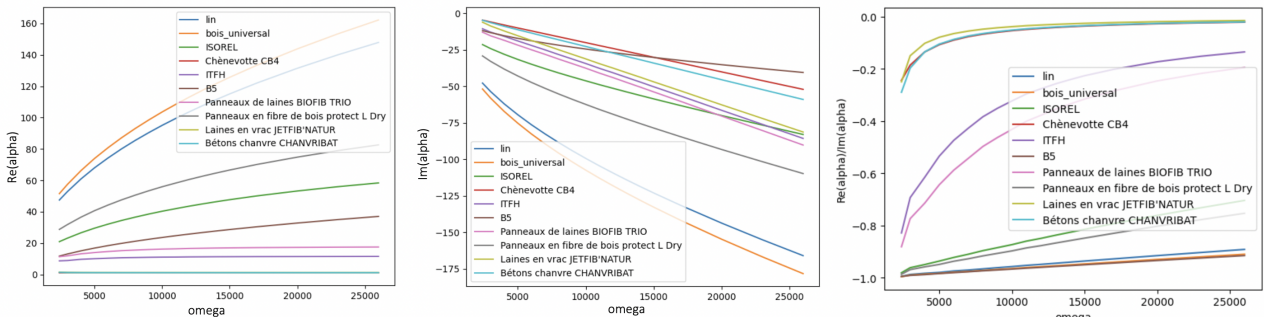


Figure 3.6: Results on $\left| \frac{\Re(\alpha)}{\Im(\alpha)} \right|$ depending on the used material for a high-frequency system

We notice that the values reached by $\Re(\alpha)$ are much higher for higher frequencies (1200 Hz). It explains the difficulties which were told in the press about the issue of absorbing low-frequency noises. Absorbing aerodynamic noises seems to be much more difficult than regular noises.

Based on the graphs we have plotted, several materials can be considered to implement our acoustic barrier. These materials can be held back :

- **ISOREL** (also called Masonite), which is a type of hardboard made of steam-cooked and pressure-molded wood fibers
- the material **B5** given in the handout
- **Wood fibre boards 'Universal'** : ecological under-roof panel made of wood fibre (French wet production)
- **Wood fibre boards Protect L Dry** : rigid wood fibre panel, produced in a dry process

Without much information on material B5 (the material designed by the authors of the document from which Figure 3.4 in the handout is taken), we give up on this approach as we would be unable to design this material. All the other materials are commercially available and we will base our study on them. In the context of a real start-up, it would have been interesting to find the designers of the material to study with them the working conditions in the manufacture of this material. In any case, we can concentrate our study on the 3 remaining materials which have similar absorption capacities.

3.2.2 Availability of the materials

In order to choose which material to use for our acoustic barrier, we can study other characteristics among the 3 remaining materials, especially on the availability of these materials. In the logic of our start-up, we consider two different points. In order to be cost-effective, we have to look at the cost of all the materials. However, we also have to consider the environmental cost of these products. The table below summarises these various elements.

Materials	ISOREL	Wood boards 'Universal'	Wood boards 'Protect L Dry'
Price (per s)	7,70 €	10,12 €	22,30 €
Composition	Softwood Fiber	Rigid Wood Fiber, Paraffin, and Aluminum Sulfate	Wood Fiber, Polyurethane Resin, and Paraffin
Environmental impact	++	-	--

Table 3.1: Price and composition analysis, given according to the same producer ([8],[10] and [9])

The analysis of the composition of the different materials leads to an (arbitrary) evaluation of the environmental impact of the considered material. The three remaining materials are composed of wood fibers, the difference relies on the other chemical species and their conception. The order given in the table relies mainly on the toxicity of aluminum sulfate and polyurethane resin(in the conception and the end of life), and also on the difficulty of recycling paraffin and polyurethane resin.

Obviously, the order given is fully arbitrary (especially between 'Universal' and 'Protect L Dry'), but we can still figure out that ISOREL stands out from the other two materials due to its composition (only bio-sourced elements). Moreover, it costs significantly much less than the other materials. All

these analysis gives us the conclusion that **ISOREL appears to be the best material to use for our acoustic barrier.**

For all the next parts, we will use ISOREL as our materials. Thus, α will be calculated using the physical parameters of ISOREL. These are the porosity $\Phi = 0, 70$, the tortuosity $\alpha_h = 1, 15$ and the resistivity to the passage of air $\sigma = 142300 \text{ N.m}^{-4}.\text{s}$.

Chapter 4

Mathematical model

4.1 Introduction

The reason why our technology is optimal in all areas, be it acoustic energy, price and quality, is the fundamental mathematical rigor that we have always tried to maintain. Let us therefore explain the mathematical background behind our solution. That is, we will explain which damping α , which quantity β of porous ISOREL material and which shape Γ minimize the acoustic energy of our solution, and hence maximize your acoustic experience. More precisely, we will explain which methods we implemented to

- model the physical phenomenon, including the noise source g ;
- optimize the damping parameter α of the system;
- optimize the porous material distribution χ ;
- optimize the fractal generation and hence the geometry of Γ ;
- optimize the porous material quantity β .

4.2 Formalization of the problem

We model the situation in the worst-case scenario, for a reflexive tunnel. In this case, for $\Omega =]0, 1[\times]0, 2[$, we decompose the compact boundary $\partial\Omega$ in $\partial\Omega = \Gamma_{\text{Dir}} \sqcup \Gamma_{\text{Neu}} \sqcup \Gamma$. We suppose that $\partial\Omega$ is a compact d -set, on which we defined a d -measure μ where $d \in [n - 1, n[$. Let us consider the problem

$$\begin{cases} (\Delta + k^2)u = 0 \text{ sur } \Omega \\ \frac{\partial u}{\partial n} = 0 \text{ sur } \Gamma_{\text{Neu}} \\ u(x) = g(x) \text{ sur } \Gamma_{\text{Dir}} \\ \frac{\partial u}{\partial n} + \chi\alpha u = 0 \text{ sur } \Gamma \end{cases}$$

The porous material distribution χ is defined on Γ by

$$\forall x \in \Gamma, \chi(x) = \mathbb{1}_{x \in \mathcal{P}}$$

where \mathcal{P} is the subset of Γ of porous material. Our model is parametrized by a coefficient $\beta \in]0, 1[$ through the coefficient

$$\int_{\Gamma} \chi d\mu = \beta \in]0, 1[$$

by supposing that $\mu(\Gamma) = 1$.

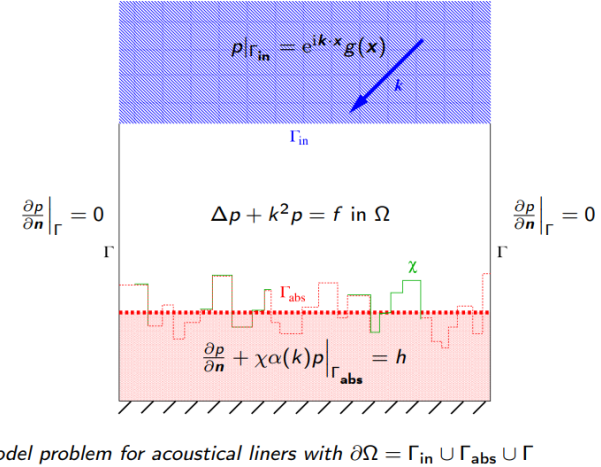


Figure 4.1: Model of the problem with notation $p := u$, $\Gamma_{\text{in}} = \Gamma_{\text{Dir}}$, $\Gamma_{\text{abs}} := \Gamma$ and $\Gamma := \Gamma_{\text{Neu}}$

The sole and the ceiling are modeled by the homogeneous Neumann boundary condition and are supposed to be reflective. The noise source is projected to the boundary Γ_{Dir} and modeled by the Dirichlet boundary condition with the function g . The perforated wall is the boundary part Γ , and it has reflective parts when $\chi = 0$ and the inclusion of a porous material if $\chi = 1$. Indeed, if $x \in \Gamma$ for which $\chi(x) = 0$, then in this point on Γ it is imposed the homogeneous Neumann boundary condition, i.e. no absorption. But if $\chi(x) = 1$, then in this point of Γ we have the Robin boundary condition

$$\frac{\partial u}{\partial n} + \alpha u = 0$$

with $\Re(\alpha) > 0$ and $\Im(\alpha) < 0$, ensuring a partial absorption and a partial reflection as explained in Chapter 3.

4.3 Determination of $\alpha(\omega)$ for a frequency ω

Note that $\alpha \in \mathbb{C}$ is a parameter that one shall determine. To do so, we will use an approach explained in [7]. The motivation consists to model the noise of the source (the function g) and, for this fixed source and a fixed porous medium, to find the coefficient α in such a way that the two problems below are equivalent. When g is a function both of space y and frequency ω , then α depends on ω as well.

$$\begin{cases} \nabla \cdot (\eta_0 \nabla u_0) + \omega^2 \epsilon_0 u_0 = 0 \text{ in } \Omega_{\text{air}} \\ \nabla \cdot (\eta_1 \nabla u_1) + \omega^2 \epsilon_1 \left(1 + \frac{\alpha i}{\xi \omega}\right) u_1 = 0 \\ \text{in } \Omega_{\text{wall}} \\ u_0 = u_1 \text{ and } \eta_0 \nabla u_0 \cdot \nu = \eta_1 \nabla u_1 \cdot \nu \text{ on } \Gamma \\ u_0(-L, y) = g(y) \text{ on the left boundary} \end{cases} \quad \begin{cases} \nabla \cdot (\eta_0 \nabla u_2) + \omega^2 \epsilon_0 u_2 = 0 \text{ in } \Omega_{\text{air}} \\ \eta_0 \nabla u_2 \cdot \nu + \alpha u_2 = 0 \text{ on } \Gamma \\ u_2(-L, y) = g(y) \text{ on the left boundary} \end{cases}$$

This approach can be better understood thanks to the following image (figure 4.2).

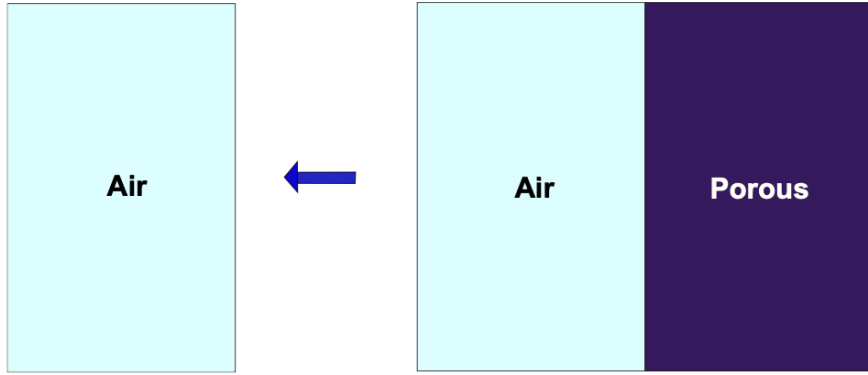


Figure 4.2: Air with boundary (left) and air with a wall composed of porous media.

Using the work fully explained in [7], one can compute $\alpha(\omega)$ as the solution of a minimization problem, see 1)

Théorème 1. Let $\Omega =] -L, L[\times] -\ell, \ell[$ be a domain with a simply connected sub-domain Ω_{air} , whose boundaries are $] -L, 0[\times \{\ell\}$, $\{-L\} \times] -\ell, \ell[$, $] -L, 0[\times \{-\ell\}$ and another boundary denoted by Γ , which is the straight line starting in $(0, -\ell)$ and ending in $(0, \ell)$. In addition, let Ω_{wall} be the supplementary domain of Ω_{air} so that Γ is the common boundary of Ω_{air} and Ω_{wall} . The length L is supposed to be large enough.

Let the original problem (the frequency version of the wave damped problem) be :

$$\begin{aligned} -\nabla \cdot (\eta_0 \nabla u_0) - \omega^2 \xi_0 u_0 &= 0 \text{ on } \Omega_{\text{air}} \\ -\nabla \cdot (\eta_1 \nabla u_1) - \omega^2 \tilde{\xi}_1 u_1 &= 0 \text{ on } \Omega_{\text{wall}} \end{aligned}$$

with $\tilde{\xi}_1 = \xi_1 \left(1 + \frac{ai}{\xi_1 \omega} \right)$ together with the boundary conditions $u_0 = u_1$ and $\eta_0 \nabla u_0 \cdot \nu = \eta_1 \nabla u_1 \cdot \nu$ on Γ and the condition on the left boundary $u_0(-L, y, \omega) = g(y, \omega)$ and some other boundary conditions. Let the modified problem be $-\nabla \cdot (\eta_0 \nabla u_2) - \omega^2 \xi_0 u_2 = 0$ on Ω_{air} with boundary absorption condition $\eta_0 \nabla u_2 \cdot \nu + \alpha u_2 = 0$ on Γ and the condition on the left boundary $u_2(-L, y, \omega) = g(y, \omega)$. Let u_0, u_1, u_2 and $g(y, \omega)$ be decomposed into Fourier modes in the y direction, denoting by k the associated wave number. Hence, ω is a parameter in the decomposition. Then the complex parameter α , minimizing the following expression

$$A \|u_0 - u_2\|_{L^2(\Omega_{\text{air}})}^2 + B \|\nabla(u_0 - u_2)\|_{L^2(\Omega_{\text{air}})^2}^2$$

can be found from the minimization with respect to α of the error function

$$e(\alpha, \omega) := \sum_{k=n\pi/L, n \in \mathbb{Z}} e_k(\alpha, \omega)$$

where e_k are given by

- if $k^2 \geq \xi_0 \omega^2 / \eta_0$:

$$\begin{aligned} e_k(\alpha, \omega) &= (A + B|k|^2) \left[\frac{1}{2\lambda_0} (|\chi|^2 (1 - e^{-2\lambda_0 L}) + |\gamma|^2 (e^{2\lambda_0 L} - 1)) + 2L \Re(\chi \bar{\gamma}) \right] \\ &\quad + B \frac{\lambda_0}{2} (|\chi|^2 (1 - e^{-2\lambda_0 L}) + |\gamma|^2 (e^{2\lambda_0 L} - 1)) - 2B\lambda_0^2 L \Re(\chi \bar{\gamma}). \end{aligned}$$

- if $k^2 < \xi_0\omega^2/\eta_0$:

$$e_k(\alpha, \omega) = (A + B|k|^2) \left[L(|\chi|^2 + |\gamma|^2) + \frac{i}{\lambda_0} \Im(\chi \bar{\gamma} (1 - e^{-2\lambda_0 L})) \right] + BL|\lambda_0|^2 (|\chi|^2 + |\gamma|^2) \\ + iB\lambda_0 \Im(\chi \bar{\gamma} (1 - e^{-2\lambda_0 L}))$$

in which $f(x) = (\lambda_0\eta_0 - x)e^{-\lambda_0 L} + (\lambda_0\eta_0 + x)e^{\lambda_0 L}$ and

$$\chi(k, \alpha, \omega) = g_{k,\omega} \left(\frac{\lambda_0\eta_0 - \lambda_1\eta_1}{f(\lambda_1\eta_1)} - \frac{\lambda_0\eta_0 - \alpha}{f(\alpha)} \right) \\ \gamma(k, \alpha, \omega) = g_{k,\omega} \left(\frac{\lambda_0\eta_0 + \lambda_1\eta_1}{f(\lambda_1\eta_1)} - \frac{\lambda_0\eta_0 + \alpha}{f(\alpha)} \right)$$

where $g_{k,\omega}$ is the Fourier coefficient of g_ω for g_ω : $y \mapsto g(y, \omega)$ at wavenumber k and

$$\lambda_0 = \sqrt{k^2 - \xi_0\omega^2/\eta_0} \text{ if } k^2 \geq \xi_0\omega^2/\eta_0 \\ \lambda_0 = i\sqrt{\xi_0\omega^2/\eta_0 - k^2} \text{ if } k^2 < \xi_0\omega^2/\eta_0$$

and

$$\lambda_1 = \frac{1}{\sqrt{2}} \sqrt{k^2 - \frac{\xi_1}{\eta_1}\omega^2 + \sqrt{\left(k^2 - \frac{\xi_1}{\eta_1}\omega^2\right)^2 + \left(\frac{a\omega}{\eta_1}\right)^2}} - \frac{i}{\sqrt{2}} \sqrt{\frac{\xi_1}{\eta_1}\omega^2 - k^2 + \sqrt{\left(\frac{\xi_1}{\eta_1}\omega^2 - k^2\right)^2 + \left(\frac{a\omega}{\eta_1}\right)^2}}.$$

The case $A = 1, B = 1$ can be considered. It is important to notice that we chose $\Omega =]0, 1[\times]0, 2[$. Hence, for the computation, this is equivalent to taking $] - 1/2, 1/2[\times] - 1, 1[$ in theorem 1, which has been done in the numerical computation.

4.4 Dirichlet condition

As seen before, the damping coefficient α requires the knowledge of the noise source g , that defines the Dirichlet boundary condition on Γ_{Dir} . We adopted several strategies to determine g , which are delineated below.

First try

We want to model the fact that there are two sources of noise (see figure 4.3):

- the aerodynamic noise of the train, modelled as a spherical wave with origin $x = 0.5$ (here we see the train as a point), initial amplitude $A_1(\omega)$ and decreasing in $\frac{1}{r}$.
- Rolling noise, modelled as a spherical wave with origin $x = 0$ (the train is no longer seen as a point and the noise comes from the wheels), initial amplitude $A_2(\omega)$ and decreasing in $1/r$.

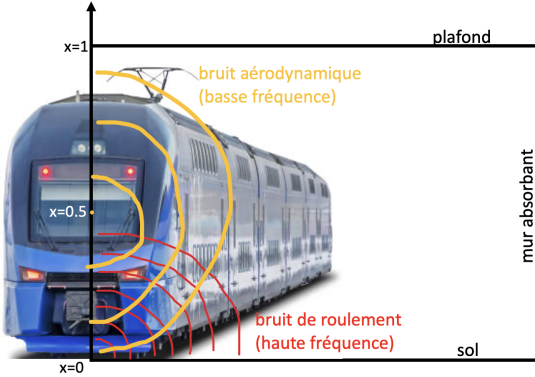


Figure 4.3: Tunnel noise modelling

We therefore take g of the following form:

$$g(\omega, x) = A_1(\omega) \frac{1}{x - 0.5} \sin\left(\frac{\omega}{c}(x - 0.5)\right) + A_2(\omega) \frac{1}{x} \sin\left(\frac{\omega}{c}x\right)$$

where c is the speed of sound in air. It remains to determine the amplitudes $A_1(\omega)$ and $A_2(\omega)$. We want to model the fact that $A_1(\omega)$ is large at low frequencies, for $\omega \in [200, 1000]$, and negligible elsewhere. We then choose A_1 such that $A_1(\log_{10}(\omega))$ is a Gaussian. The same applies to A_2 . We want to take large values for $\omega \in [2500, 25000]$. Furthermore, for speeds of around 320 km/h, Figure 3.1 shows a difference of about 3dB between the two noises. We therefore take the maximum value of A_2 to be half that of A_1 .

Finally, we take

$$A_1(\omega) = \exp\left(-\frac{(\log_{10}\omega - \mu_1)^2}{2\sigma_1^2}\right)$$

and

$$A_2(\omega) = \exp\left(-\frac{(\log_{10}\omega - \mu_2)^2}{2\sigma_2^2}\right),$$

with $\mu_1 = 2.64$, $\sigma_1 = 0.156$, $\mu_2 = 3.88$ and $\sigma_2 = 0.204$, so as to have the following graph 4.4 for A_1 , A_2 :

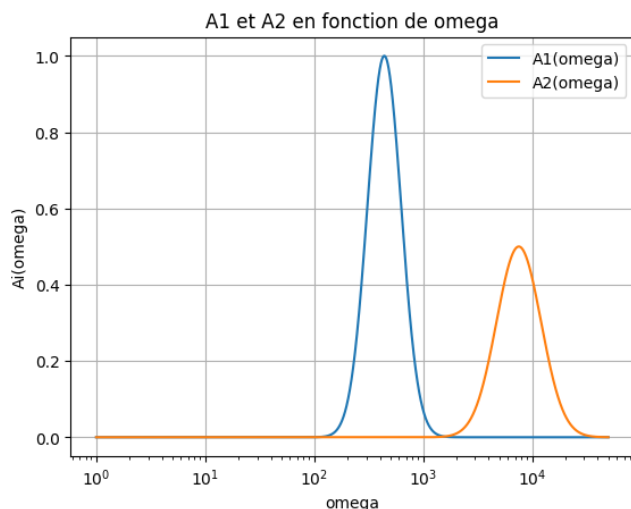


Figure 4.4: $A_1(\omega)$ et $A_2(\omega)$

Due to irregularities in this model, shown in figure 4.5 concerning $\Re(\alpha)$ and $\Im(\alpha)$ that are supposed to be regular (in $C^0(\Omega)$ at least), we opted for another modelization of the noise source g .

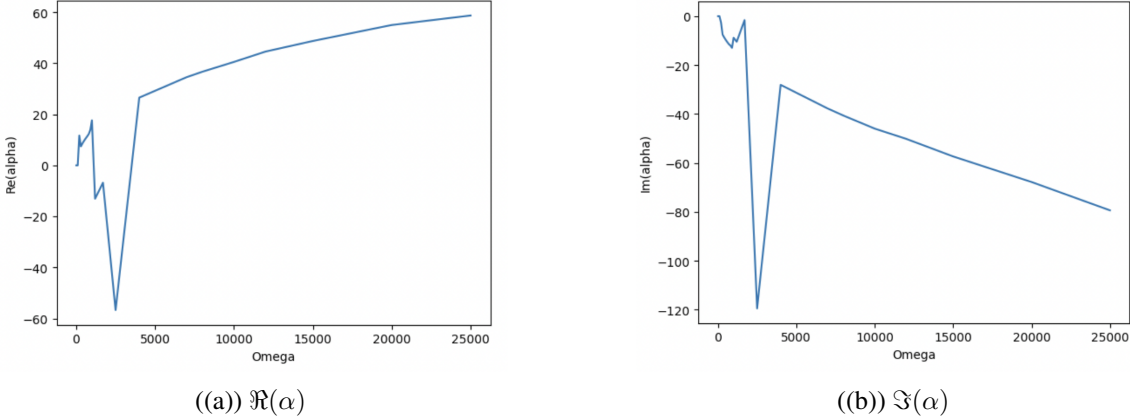


Figure 4.5: Real and imaginary parts of α for the ISOREL material, calculated with the g function under consideration

In fact, our algorithm works for

$$g(\omega, x) = \frac{\omega}{c} \text{sinc}\left(\frac{\omega}{c}(x - 0.5)\right) + \frac{\omega}{c} \text{sinc}\left(\frac{\omega}{c}x\right).$$

We deduce that it is the coefficients $A_1(\omega)$ and $A_2(\omega)$ that pose a problem, although we are unable to explain why.

Second try

We choose a simpler model of the problem: we model the fact that the train emits noise over a range of frequencies, for $\omega \in \underline{\omega} := [100, 700]$ and for $\omega \in a\underline{\omega} + b$, and that the noise emitted over the first frequency is twice as loud, where $a = 37.5$ and $b = -1250 \text{ rad.s}^{-1}$. We no longer model the spatial position of the noise sources, instead we consider that the noise is distributed in space according to a Gaussian centred at $\mu_0 = 0.5$ and of variance $\sigma_0 = 1$. Finally, we take :

$$g(x) = \exp\left(-\frac{(x - \mu_0)^2}{2\sigma_0^2}\right) \left(2 \sin\left(\frac{\omega}{c}x\right) + \sin\left(\frac{a\omega + b}{c}x\right)\right)$$

The results obtained for this g function are more consistent. We can plot the α graph obtained with this new function (see figure 4.6).

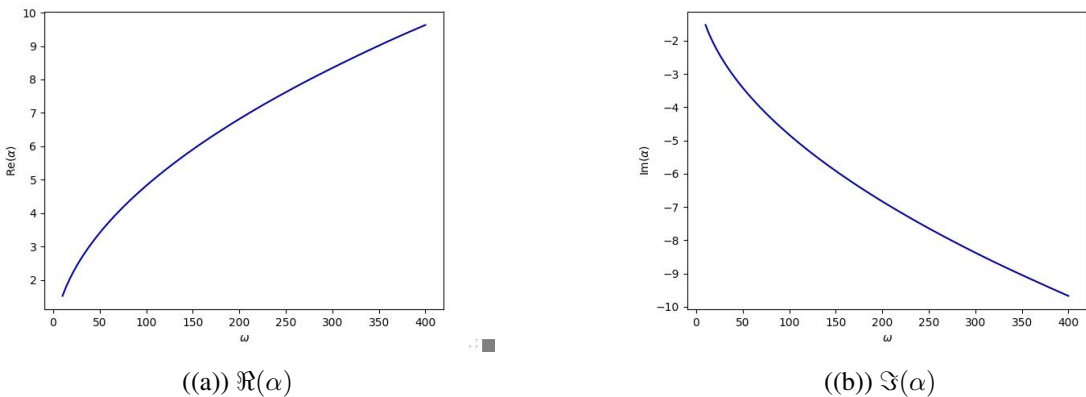


Figure 4.6: Real and imaginary parts of α for the ISOREL material, calculated with the g function under consideration

The error $e(\alpha, \omega)$ induced by the numerical approximation is represented below in plot 4.7.

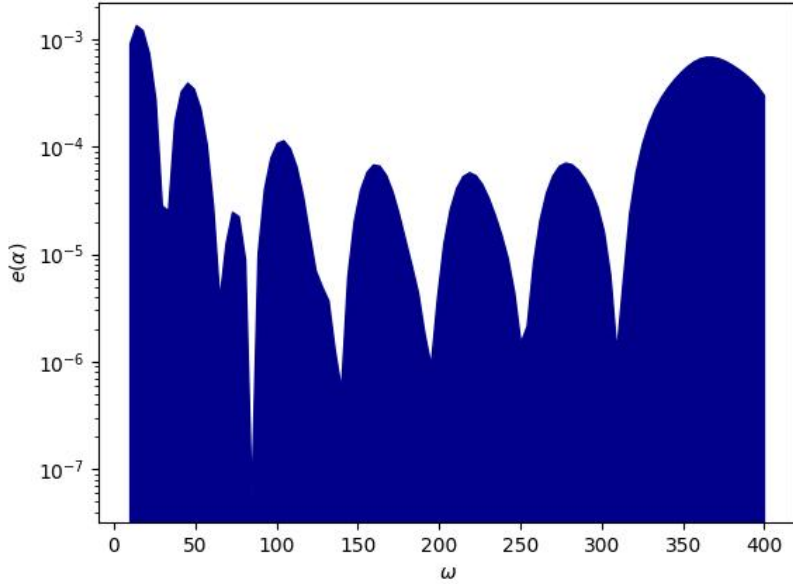


Figure 4.7: Error $e(\alpha, \omega)$ for ISOREL material

From now on, we will consider this function g for the Dirichlet condition.

4.5 Optimizing the distribution of acoustic energy

The goal is to find $\chi \in L^\infty(\Gamma, \mu)$ such as the acoustic energy

$$J(\chi) := \int_{\Omega} |u(\chi)|^2 dx$$

is minimal, when $u(\chi)$ is the solution of:

$$\begin{cases} (\Delta + k^2)u = f \text{ sur } \Omega \\ \frac{\partial u}{\partial n} = 0 \text{ sur } \Gamma_{\text{Neu}} \\ u(x) = g(x) \text{ sur } \Gamma_{\text{Dir}} \\ \frac{\partial u}{\partial n} + \chi \alpha u = 0 \text{ sur } \Gamma \end{cases}$$

To solve this problem, we consider χ to require minimal conditions, already mentioned, such that $\chi \in U_{\text{ad}}(\beta)$ defined below :

$$U_{\text{ad}}(\beta) = \left\{ \chi \in L^\infty(\Gamma_{\text{abs}}); \forall x \in \Gamma, \chi(x) \in \{0, 1\}, \int_{\Gamma} \chi d\mu = \beta \right\}.$$

As $U_{\text{ad}}(\beta)$ is not compact for the weak* convergence in $L^\infty(\Gamma, \mu)$, we rather consider its convex closure for the aforementioned convergence. It is denoted $U_{\text{ad}}^*(\beta)$ and is defined by

$$U_{\text{ad}}^*(\beta) = \left\{ \chi \in L^\infty(\Gamma_{\text{abs}}); \forall x \in \Gamma, \chi(x) \in [0, 1], \int_{\Gamma} \chi d\mu = \beta \right\} \supseteq U_{\text{ad}}(\beta).$$

It can be shown that for Γ, f, g, k, α sufficiently well defined on our domain $\Omega \subset \mathbb{R}^2$, then for a fixed $\beta \in]0, \mu(\Gamma)[$ there exists an optimal distribution $\hat{\chi} \in U_{\text{ad}}^*(\beta)$ and an optimal solution $u(\hat{\chi}) \in V(\Omega)$ such that

$$J^*(\hat{\chi}) = \min_{\chi \in U_{\text{ad}}^*(\beta)} J^*(\chi) = \inf_{\chi \in U_{\text{ad}}(\beta)} J(\chi).$$

Our objective is therefore to find an approximation of $\pi(\hat{\chi}) \in U_{\text{ad}}(\beta)$ minimizing J , where $\pi: U_{\text{ad}}^*(\beta) \rightarrow U_{\text{ad}}(\beta)$ is the projection. Considering multiple shapes, we will then find the optimal shape.

To do so, we will use a gradient descent algorithm, requiring the Fréchet energy derivative and the projection. First, we use algorithm to compute the final projection $\pi: U_{\text{ad}}^*(\beta) \rightarrow U_{\text{ad}}(\beta)$.

Algorithm 1 Projection $\pi: U_{\text{ad}}^*(\beta) \rightarrow U_{\text{ad}}(\beta)$

```

1: function PROJECTION_FINAL( $\chi, V_{\text{obj}}$ , domain_omega)
2:   table  $\leftarrow []$ 
3:    $M, N \leftarrow \text{shape}(\chi)$ 
4:    $S \leftarrow 0$  ▷ Surface du fractal
5:   for  $i \leftarrow 1$  to  $M$  do
6:     for  $j \leftarrow 1$  to  $N$  do
7:       if domain_omega[ $i, j$ ] == _env.NODE_ROBIN then
8:         table.append(( $\chi[i, j], (i, j)$ ))
9:          $S \leftarrow S + 1$ 
10:      end if
11:    end for
12:  end for
13:  table.sort(reverse=True)
14:   $\chi_1 \leftarrow \text{zeros}(M, N)$ 
15:  nbre_de_uns  $\leftarrow \text{int}(V_{\text{obj}} \times S)$ 
16:   $i \leftarrow 1$ 
17:  while  $i < \text{nbre\_de\_uns}$  do
18:    value, node_id  $\leftarrow \text{table}[i]$ 
19:    node_i, node_j  $\leftarrow \text{node\_id}$ 
20:     $\chi_1[\text{node\_i}, \text{node\_j}] \leftarrow 1$ 
21:     $i \leftarrow i + 1$ 
22:  end while
23:  return  $\chi_1$ 
24: end function

```

The Fréchet derivative of $J(\chi)$ is the linear form $J'(\chi) : L^\infty(\Gamma, \mu) \rightarrow \mathbb{R}$ such that

$$J(\chi + h) = J(\chi) + J'(\chi)(h) + \|h\|_{L^\infty(\Gamma, \mu)} \epsilon(h)$$

for $\epsilon: L^\infty(\Gamma, \mu) \rightarrow \mathbb{R}$ such that $\lim_{h \rightarrow 0} |\epsilon(h)| = 0$.

Théorème 2. *The cost function $J(\chi) = \int_\Omega |u(\chi)|^2 dx$ is Fréchet-differentiable and*

$$J'(\chi): \chi_0 \in L^\infty(\Gamma, \mu) \mapsto - \int_\Gamma \chi_0 \Re(\alpha u(\chi) p(\chi)) d\mu,$$

where $p(\chi)$ is the solution of the adjoint problem defined below

$$\begin{cases} (\Delta + k^2)p = -2\bar{u}(\chi) \text{ in } \Omega, \\ p = 0 \text{ on } \Gamma_{\text{Dir}}, \\ \frac{\partial p}{\partial n} = 0 \text{ on } \Gamma_{\text{Dir}}, \\ \frac{\partial p}{\partial n} + \alpha\chi p = 0 \text{ on } \Gamma. \end{cases}$$

Numerically, $\chi \in U_{\text{ad}}^*(\beta)$ is obtained by gradient descent algorithm 2, using the following projection, since $\chi_n - \mu_n J'(\chi_n) \in \mathcal{F}(\Gamma, \mathbb{R})$ must still be projected into $U_{\text{ad}}(\beta)$ to define χ_{n+1} :

$$\mathcal{P}_\ell: \chi \in \mathcal{F}(\Gamma, \mathbb{R}) \mapsto \max(0, \min(\chi + \ell, 1)) \in U_{\text{ad}}(\beta)$$

The algorithm is ended after K iterations. In our computation, we fix $K := \text{numb_iter} = 100$.

Algorithm 2 Gradient descent algorithm

Require: $\chi_0 \in U_{\text{ad}}(\beta), \mu_0 \in \mathbb{R}_+^*, (\epsilon_0, \epsilon_1, \epsilon_2, \epsilon_3) \in \mathbb{R}_+^*$ ⁴

for $k \in \llbracket 0, K \rrbracket$ **do**

 Compute $u(\chi_k), p(\chi_k), J(\chi_k), J'(\chi_k)$

$E = J(\chi_k)$

while $E \geqslant J(\chi_k) \& \mu > \epsilon_0$ **do**

$\ell = 0$

$\chi_{k+1} = \mathcal{P}_\ell(\chi_k - \mu J'(\chi_k))$

while $\left| \int_\Gamma \chi_{k+1} d\mu - \beta \right| \geqslant \epsilon_1$ **do**

if $\int_\Gamma \chi_{k+1} d\mu \geqslant \beta$ **then**

$\ell \leftarrow \ell - \epsilon_2$

else

$\ell \leftarrow \ell + \epsilon_2$

end if

$\chi_{k+1} = \mathcal{P}_\ell(\chi_k - \mu J'(\chi_k))$

end while

 Compute $u(\chi_{k+1}), J(\chi_{k+1})$

$E = J(\chi_{k+1})$

if $E < J(\chi_k)$ **then**

$\mu \leftarrow \mu + \epsilon_3$

else

$\mu \leftarrow \mu/2$

end if

end while

end for

4.6 Open-air boundary theoretical study

Let us consider that one boundary is open-air (the wave go through without coming back). To model the open-air type of boundaries, it is convient to consider the Sommerfeld radiation condition of the form

$$\frac{\partial v}{\partial n} - ik \operatorname{Tr} v = 0$$

with the notation $u(x, t) = e^{-ikx}v(x, t)$ for the propagative wave. We therefore can decompose $\partial\Omega$ in the following form

$$\partial\Omega = \Gamma_{\text{Dir}} \sqcup \Gamma_{\text{Neu}} \sqcup \Gamma_S \sqcup \Gamma$$

where Γ_S is the Sommerfeld boundary. The problem hence writes

$$\left\{ \begin{array}{l} (\Delta + k^2)u = 0 \text{ sur } \Omega \\ \frac{\partial u}{\partial n} = 0 \text{ sur } \Gamma_{\text{Neu}} \\ \frac{\partial u}{\partial n} - iku = 0 \text{ sur } \Gamma_S \\ u(x) = g(x) \text{ sur } \Gamma_{\text{Dir}} \\ \frac{\partial u}{\partial n} + \chi\alpha u = 0 \text{ sur } \Gamma \end{array} \right.$$

Let us write $u = \hat{u} + \hat{g}$. By stating $f = f - k^2\hat{g}$, $\eta_1 = -\alpha\chi\hat{g}$ and $\eta_2 = ik\hat{g}$, one can transform this problem into the problem on \hat{u} :

$$\left\{ \begin{array}{l} (\Delta + k^2)\hat{u} = f \text{ sur } \Omega \\ \frac{\partial \hat{u}}{\partial n} = 0 \text{ sur } \Gamma_{\text{Neu}} \\ \frac{\partial \hat{u}}{\partial n} - ik\hat{u} = \eta_1 \text{ sur } \Gamma_S \\ \hat{u}(x) = 0 \text{ sur } \Gamma_{\text{Dir}} \\ \frac{\partial \hat{u}}{\partial n} + \chi\alpha\hat{u} = \eta_2 \text{ sur } \Gamma \end{array} \right.$$

Let us write the variational formulation associated to this problem. For $\varphi \in V(\Omega)$, by using the formula

$$\left\langle \frac{\partial \hat{u}}{\partial n}, \text{Tr } \varphi \right\rangle_{(B'(\partial\Omega), B(\partial\Omega))} = \int_{\Omega} \nabla \hat{u} \nabla \bar{\varphi} dx + \int_{\Omega} \Delta \hat{u} \bar{\varphi} dx$$

we have

$$\begin{aligned} & -(\hat{u}, \varphi)_{L^2(\Omega)} + k^2(\hat{u}, \varphi)_{L^2(\Omega)} + (\eta_2, \text{Tr } \varphi)_{L^2(\Gamma)} + (\eta_1, \text{Tr } \varphi)_{L^2(\Gamma_S)} \\ & + ik(\text{Tr } \hat{u}, \text{Tr } \varphi)_{L^2(\Gamma_S)} - \alpha(\text{Tr } (\chi\hat{u}), \text{Tr } \varphi)_{L^2(\Gamma)} + (f, \varphi)_{L^2(\Omega)} = 0 \end{aligned}$$

We then define the Lagrangian by $\mathcal{L}(\chi, w, q) = FV(\chi, w, q) + J(\chi)$ where $FV(\chi, \hat{u}(\chi), q) = 0$ for all $q \in V(\Omega)$. By the course, we have

$$\langle J'(\chi), \chi_0 \rangle = \left\langle \frac{\partial FV}{\partial \chi}(\chi, \hat{u}(\chi), \hat{p}(\chi)), \chi_0 \right\rangle.$$

But, by definition of $FV(\chi, \hat{u}(\chi), \hat{p}(\chi))$, it's derivative with respect to χ yields

$$J'(\chi) = -\alpha \Re(\hat{u}(\chi) \hat{p}(\chi)).$$

Thus, the derivative of the energy over the distribution remains the same. One can therefore very well suppose the upper boundary to be closed.

4.7 Optimizing β using LASSO regression and the wall shape

As we want to take into account both the minimization of acoustic energy $J(\chi_\beta)$ and of β (as porous material is generally more expensive than the fully reflective one), we choose a hyper-parameter λ parameterizing the penalization by β .

Hence, the result of our study can be formalized by the following optimization problem :

$$(\hat{n}, \hat{\beta}) \in \arg \min_{\substack{n \in \mathbb{N} \\ \beta \in [0,1]}} J\left(\hat{\chi}_{\beta}^{(n)}\right) + \lambda \beta.$$

Here, $\hat{\chi}_{\beta}$ corresponds to the approximation of the optimal distribution by algorithm 2. Intuitively, we will select the generation and quantity where the overall energy is the least. Also, should we have

$$\#\left(\arg \min_{\beta \in [0,1]} J\left(\hat{\chi}_{\beta}^{(\hat{n})}\right)\right) > 1,$$

then we will simply take

$$\hat{\beta} = \inf \left(\arg \min_{\beta \in [0,1]} J\left(\hat{\chi}_{\hat{\beta}}^{(\hat{n})}\right) \right)$$

in order to minimize the cost.

Chapter 5

Numerical results

5.1 Optimizing β and fractal shape

We compare the density of energy in the domain without our solution and with our solutions and see the efficiency with a decrease in energy. As explained in chapter 4, we have first investigated the optimization of hyper-parameter $\lambda > 0$. Figure 5.1 shows the influence of λ on the objective function.

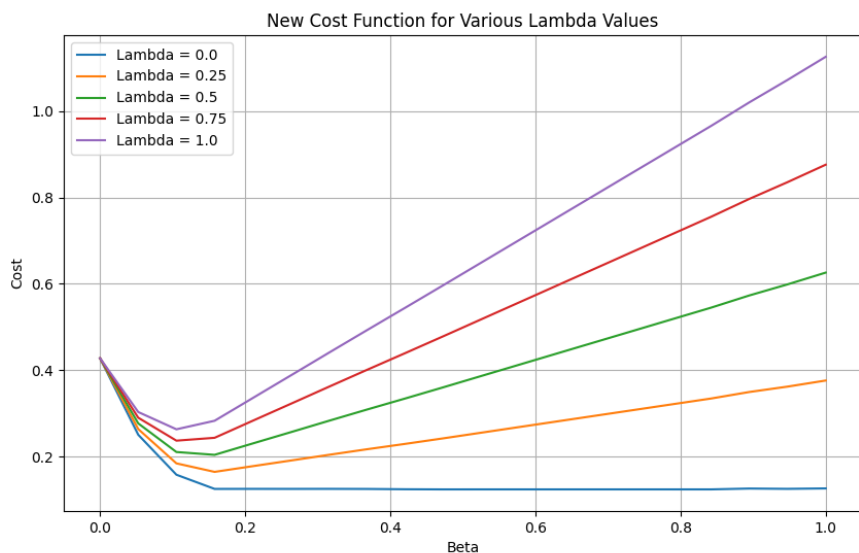


Figure 5.1: Influence of hyper-parameter λ on cost function

One can infer that for increasing values of β , the graphs tend to diverge one from another and cost becomes more important. Consequently, it becomes increasingly interesting to opt for a complex geometry of Γ , as the acute localization of acoustic energy allows for less porous material. Also, if we denote \mathcal{C}_λ the graph associated to hyper-parameter λ for a fixed fractal generation, then $\lambda \mapsto \mathcal{C}_\lambda$ is increasing, by assuming that $\mathcal{C}_{\lambda_1} \preccurlyeq \mathcal{C}_{\lambda_2}$ means that the left term curve is totally above the right term curve. We will therefore consider $\lambda = 1$ for the upcoming computations.

That is, we obtain the following plot 5.2.

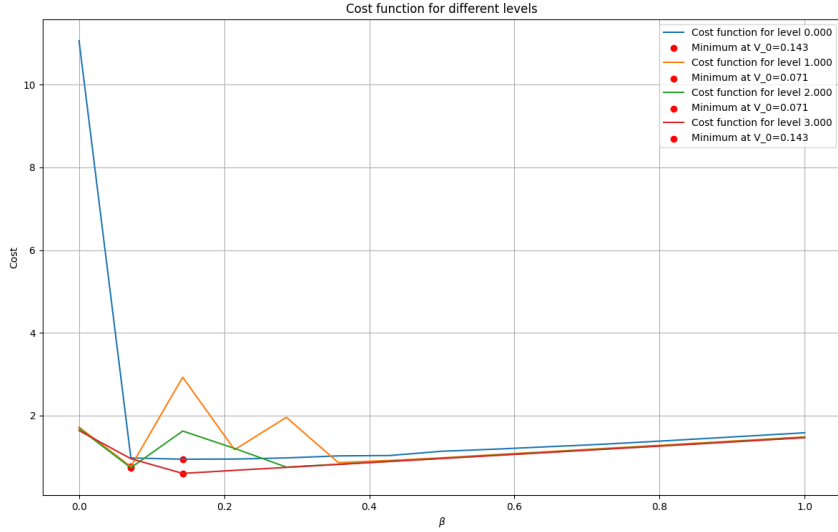


Figure 5.2: Determination of $(\hat{n}, \hat{\beta})$

This study permits to conclude that the acoustic wall will consist of a fraction $\hat{\beta} = 14\%$ of porous material, forming a Von Koch pre-fractal of generation $\hat{n} = 3$. Although one may think that 14.3% is not a lot of porous material, one should still consider that due to the high complexity of Γ geometry, the acoustic energy is way more localised, hence requiring less porous material.

The effective structure of the acoustic wall is represented on figures 5.3 and 5.4.

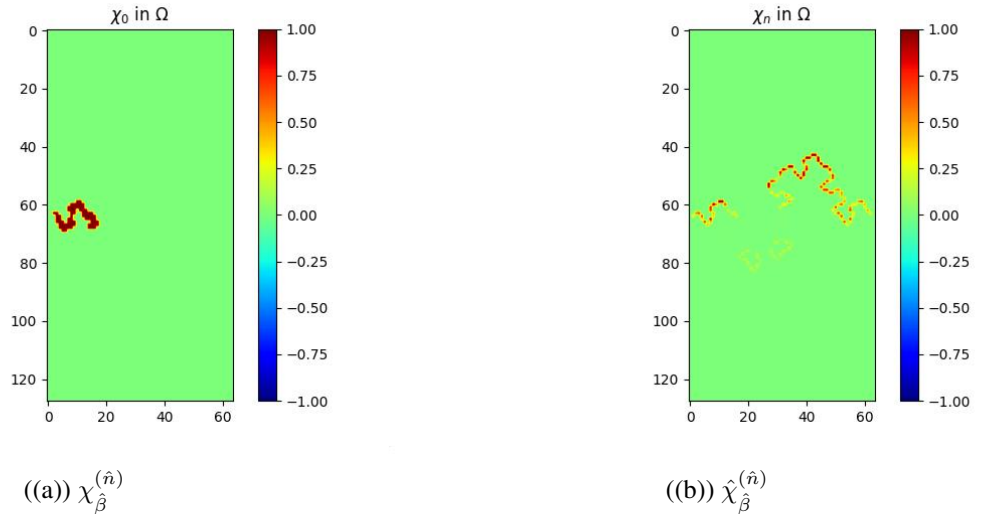


Figure 5.3: Comparison of porous material distribution before and after optimization process

Let us now examine the properties of our computation of $\hat{\chi}_{\hat{\beta}}^{(\hat{n})}$. To do so, we take a look at $\Re(u_0)$ and $\Im(u_n)$ which correspond to the solutions of our PDE for $\hat{\beta}$ and \hat{n} , respectively for $\chi = \chi_0$ and $\chi = \hat{\chi}$. Also, we study $\Im(u_0)$ and $\Im(u_n)$, which allows to look at the error $\Re(u_n - u_0)$ and $\Im(u_n - u_0)$.

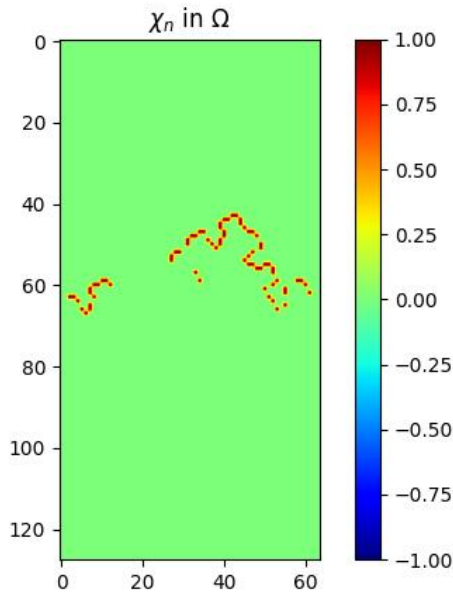


Figure 5.4: Projection of $\hat{\chi}_{\hat{\beta}}^{(\hat{n})}$ onto $U_{\text{ad}}(\beta)$

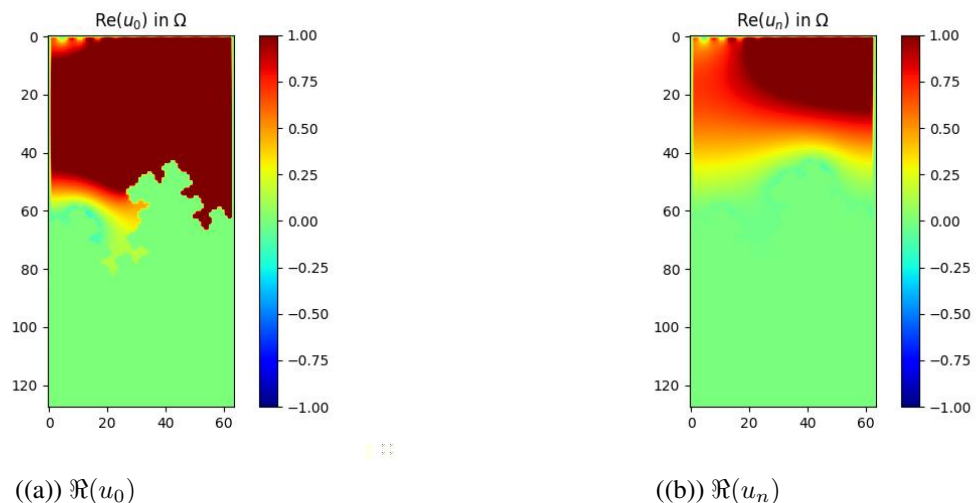


Figure 5.5: Comparison of real part of solution $u \in V(\Omega)$ before and after optimization of χ

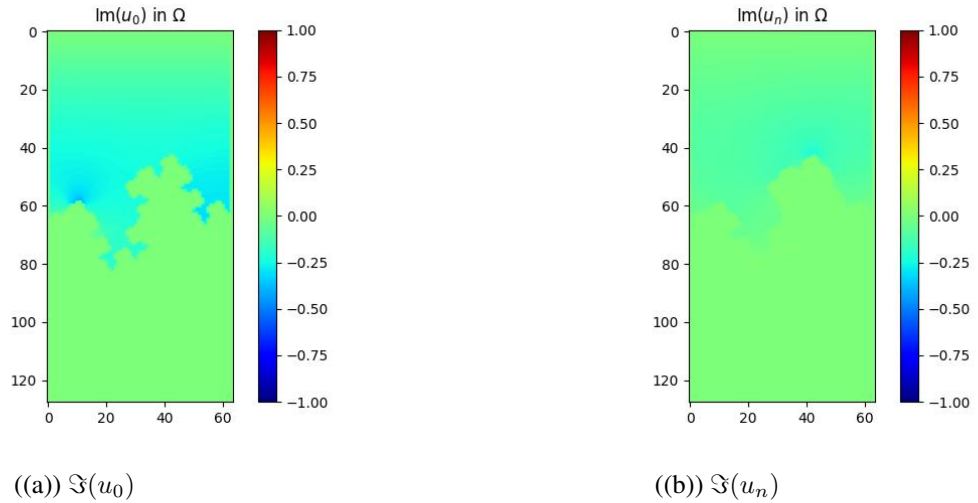


Figure 5.6: Comparison of imaginary part of solution $u \in V(\Omega)$ before and after optimization of χ

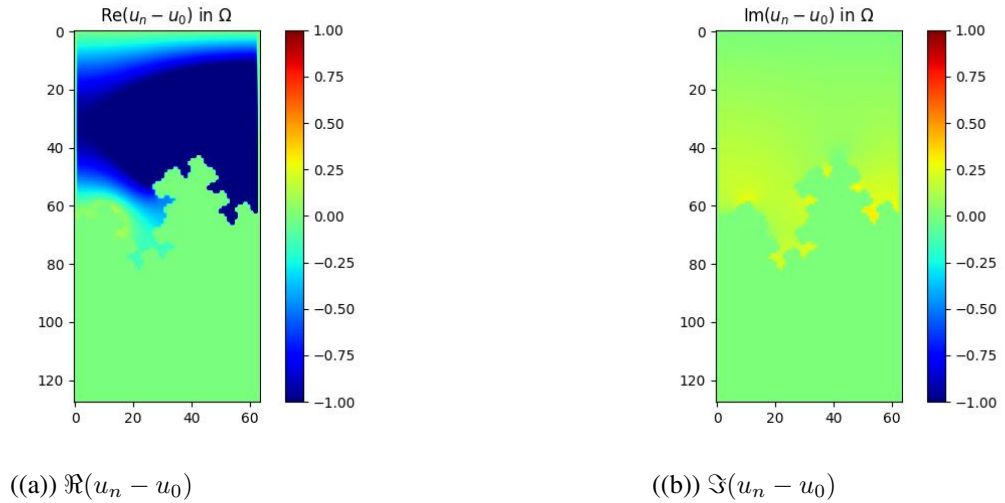


Figure 5.7: Comparison of error of imaginary part and real part

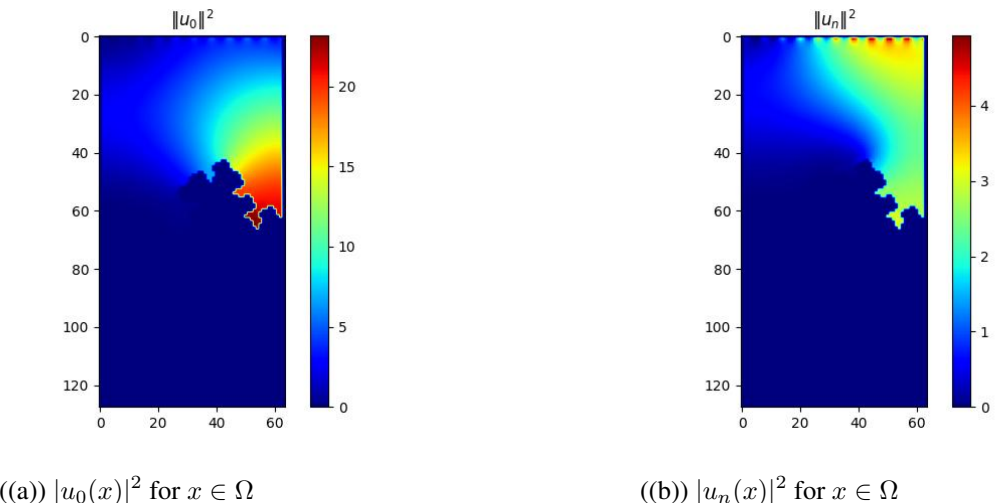


Figure 5.8: Comparison of norm of solution $u \in V(\Omega)$ before and after optimization of χ

The convergence of our energy by gradient descent is demonstrated on 5.9. The rather quick convergence proves that our algorithm works well and really permits to minimize the acoustic energy by optimizing the porous material distribution.

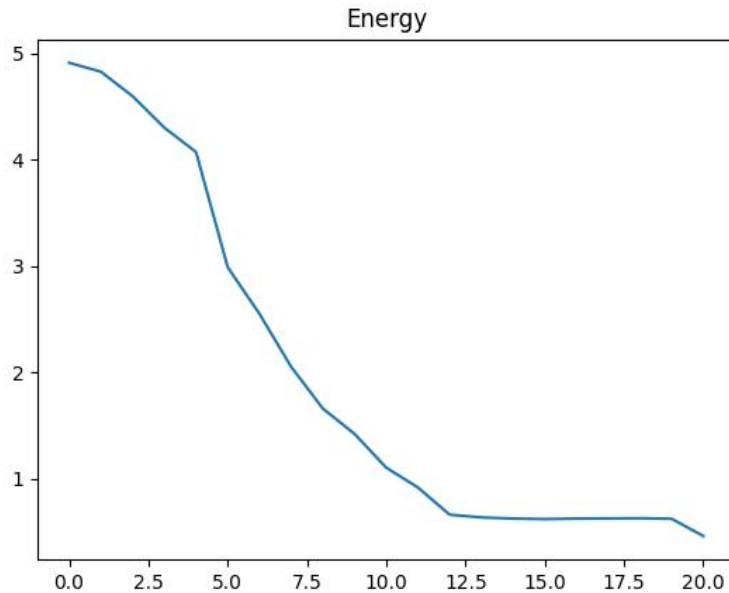


Figure 5.9: Energy $J\left(\chi_{k,\hat{\beta}}^{(\hat{n})}\right)$ when iterating k in optimization

5.2 Frequency study

It remains to be seen though, whether the distribution $\hat{\chi}$ effectively reduces the acoustic energy on the frequency domain $\underline{\omega}$ and $a\underline{\omega} + b$. We therefore compare the performance of $J(\omega)$ for three cases

- $\chi = 0$ on Γ
- $\chi = 1$ on Γ
- $\chi = \hat{\chi}$ optimised for an optimized $\hat{\beta}$ and fractal shape Γ of generation $\hat{n} = 3$.

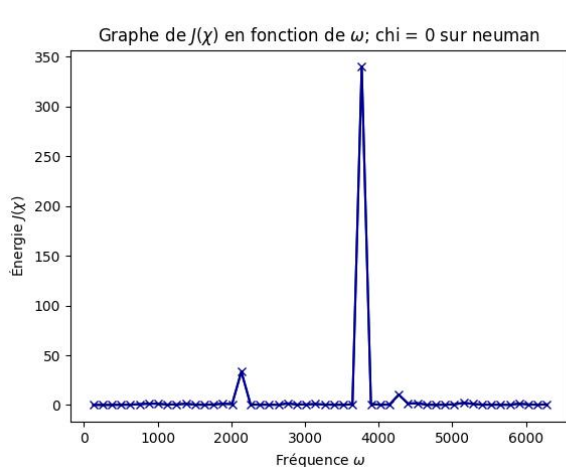


Figure 5.10: Reflexive material on a flat wall

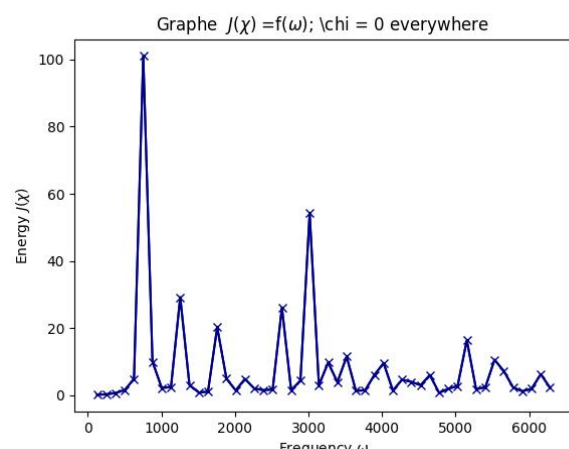


Figure 5.11: Reflexive material on a fractal wall level 3

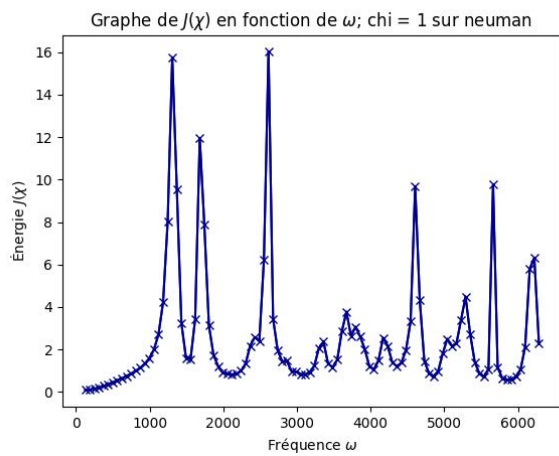


Figure 5.12: Absorbent material on a flat wall

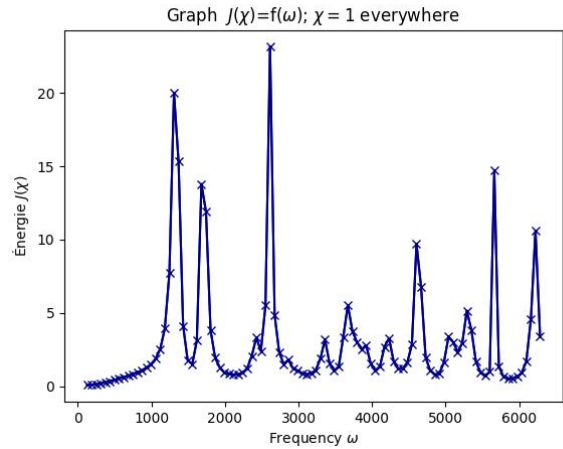


Figure 5.13: Absorbent material on a fractal wall level 3

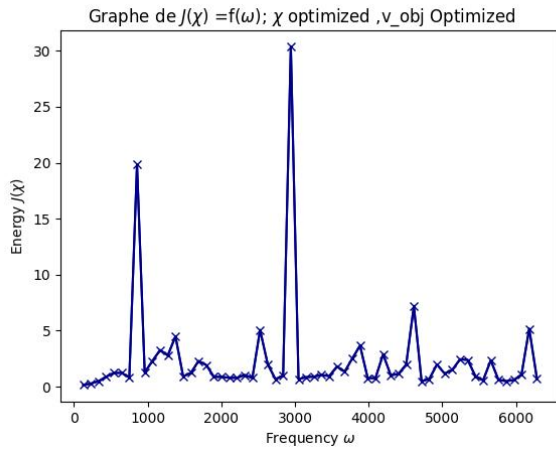
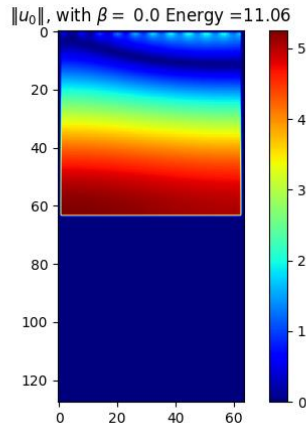


Figure 5.14: Optimized wall

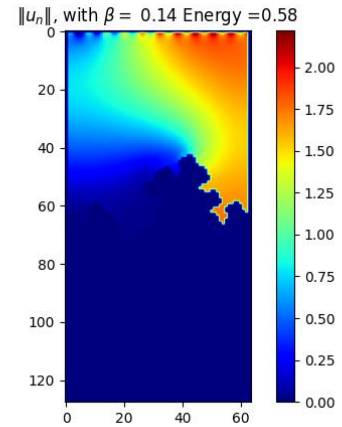
This comparison yields an effective reduction of acoustic energy on the frequency domain of interest.

5.3 Conclusion

Finally, one can examine to what extent our solution permits to reduce acoustic energy. We compare in figure 5.15 the distribution of $|u|^2$ over domain Ω respectively when there is no porous material and the wall is totally flat and when we implement our optimal solution.



((a)) $|u_0(x)|$ for $x \in \Omega$



((b)) $|u_n(x)|$ for $x \in \Omega$

Figure 5.15: Comparison of $|u|$ on Ω between $(n, \beta) = (0, 0)$ and $(\hat{n}, \hat{\beta})$ after optimization of distribution (null in first case)

To conclude, our solution permits to reduce the acoustic energy on domain Ω by a factor of $11.06/0.58 \approx 19$, which impressively underlines the efficiency of our solution.

Chapter 6

Conclusion

To conclude, we have made a comprehensive study to determine the best material for our anti-noise wall. This study, combining **absorption, price and ecological factors**, has allowed us to focus on **ISOREL, of porosity $\phi = 0,70$, tortuosity $\alpha_h = 1,15$ and resistivity $\sigma = 142300 \text{ N.s/m}^4$** . Moreover, a rigorous mathematical model and subsequent optimization methods (gradient descent, LASSO regression) permitted the optimization of the parameters of the model, that are β , the fractal generation n and finally the determination of the distribution of porous material χ . **Eventually, the acoustic wall will consist of a fraction $\hat{\beta} = 14,3\%$ of porous material, forming a Von Koch pre-fractal of generation $\hat{n} = 3$.** The acoustic wall (to be precise, the distribution of porous material) is once again represented below, on figure 6.1. **The acoustic energy is massively reduced thanks to our solution, that is by a factor of $11.06/0.58 \approx 19$.**

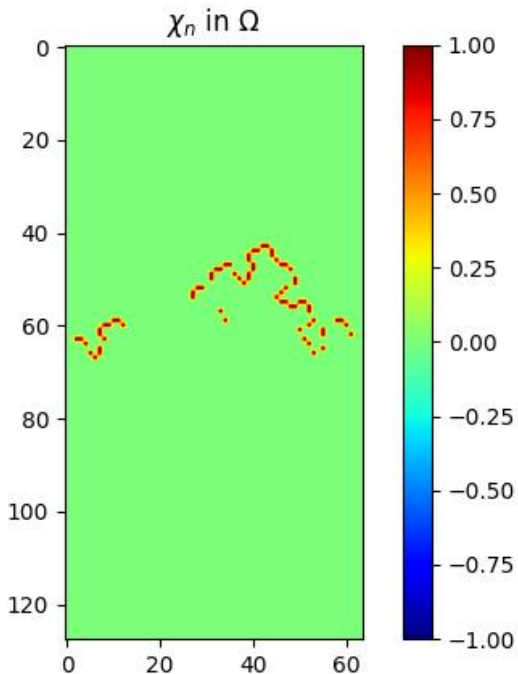


Figure 6.1: Distribution of porous material on the fractal wall

Bibliography

- [1] batiweb. *Des murs antibruit en béton de caoutchouc et bois pour la ligne Massy-Valenton.* 2014. URL: <https://www.batiweb.com/actualites/collectivites-territoriales-des-murs-antibruit-en-beton-de-caoutchouc-et-bois-pour-la-ligne-massy-valenton-25463>.
- [2] RPG Europe. *RPG Skyline.* URL: <https://www.rpgeurope.com/products/product/skyline.html>.
- [3] Fabien Letournaux Florence Margiocchi Pierre-Etienne Gautier. “Caractérisation vibro-acoustique d’une voie ferrée”. *inAcoustique et techniques:* (2006), page 1. URL: https://www.bruit.fr/images/acoustique_techniques/AT46-47-24-33_compressed.pdf.
- [4] Philippe Glé. “Acoustique des Matériaux du Bâtiment à base de Fibres et Particules Végétales - Outils de Caractérisation, Modélisation et Optimisation.” *in*(2013): pages 41–83. URL: <https://theses.hal.science/tel-00923665>.
- [5] Jean-Marc De Jaeger. “Quels sont les trains les plus rapides du monde ?” *inLe Figaro:* (2022).
- [6] Thibaut BLINET Thierry FALWISANNER Philippe GLÉ Catherine GUIGOU CARTER Elias KADRI. “PROPRIETES ACOUSTIQUES DES MATERIAUX BIOSOURCES”. *inMinistère de la transition écologique et solidaire Ministère de la cohésion des territoires:* (2017).
- [7] Frédéric Magoulès **and others**. “Optimal absorption of acoustical waves by a boundary”. *inSIAM Journal on Control and Optimization:* 59.1 (2021), pages 561–583. DOI: [10.1137/20M1327239](https://doi.org/10.1137/20M1327239). URL: <https://hal.science/hal-01558043>.
- [8] Matériaux Naturels. *STEICO Isorel - Panneau acoustique fibre de bois.* 2022. URL: <https://www.materiaux-naturels.fr/produit-decl/5670-steico-isorel-panneau-acoustique-fibre-de-bois-19mm-1350-x-600-bd>.
- [9] Matériaux Naturels. *STEICO Protect L Dry - Panneau isolant extérieur.* 2022. URL: <https://www.materiaux-naturels.fr/produit/1156-steico-protect-dry-panneau-isolant-exterieur-a-enduire>.
- [10] Matériaux Naturels. *STEICO Universal - Panneau pare pluie fibre de bois rigide.* 2022. URL: <https://www.materiaux-naturels.fr/produit/402-steico-universal-panneau-pare-pluie-fibre-de-bois-rigide>.
- [11] L’Usine Nouvelle. “Des fractales pour un mur anti-bruit”. *in*(2004): URL: <https://www.usinenouvelle.com/article/des-fractales-pour-un-mur-anti-bruit.N1973792>.
- [12] SNCF Réseaux. *Le bruit ferroviaire en questions reponses.* 2018. URL: https://it4v7.interactiv-doc.fr/html/fne_sncf_bruit_web_pdf_914/.
- [13] SNCF réseaux. *Prévenir et réduire le bruit ferroviaire.* 2022. URL: <https://www.sncf-reseau.com/fr/entreprise/newsroom/sujet/engagement-prevenir-reduire-bruit-ferroviaire>.

- [14] Strail. *STRAILastic_mSW*. 2022. URL: https://www.strail.fr/strailastic/strailastic_msw/#1564412250222-f41a9676-e2d554f5-83981138-7c35.
- [15] Xinwen Yang **and** Caiyun Yan. “Simulation of Wheel/Rail Noise of High Speed Train Running on the Slab Track”. **injuly** 2009: **pages** 1–6. ISBN: 978-0-7844-1064-6. DOI: [10.1061/\(358\)469](https://doi.org/10.1061/(358)469).